JOURNAL OF PROPULSION AND POWER
Vol. 22, No. 1, January–February 2006

Technical Notes

TECHNICAL NOTES are short manuscripts describing new developments or important results of a preliminary nature. These Notes should not exceed 2500 words (where a figure or table counts as 200 words). Following informal review by the Editors, they may be published within a few months of the date of receipt. Style requirements are the same as for regular contributions (see inside back cover).

Experimental Investigation of a Submerged Subsonic Inlet

Vasilije J. Jovanovic,* Ezgi S. Taskinoglu,† and Doyle D. Knight‡
Rutgers University, Piscataway, New Jersey 08854
and
Gregory S. Elliott§
University of Illinois at Urbana–Champaign, Urbana, Illinois 61801

Introduction

THE inlet is the component of an airbreathing vehicle that is responsible for bringing atmospheric air to a ramjet, turbojet, or turbofan engine. It is a channel in which a portion of the kinetic energy of the air per unit mass is converted to an increase in thermal energy and, hence, static pressure. It is desired that the pressure recovery of the inlet be maximized to achieve the highest level of thrust, while the nonuniformity of the airflow be maintained below a specified level to prevent compressor failure due to the blade vibration or engine surge due to boundary-layer separation. Among many designed and tested inlet types, the submerged inlet (also known as flush-mounted or hidden inlet) has several advantages compared to conventional external inlets. Because of its position within the vehicle body, a submerged inlet has lower drag and weight compared to other inlet types. Additionally, its small radar cross section yields lower observability. However, the inlet geometry and position within the air vehicle body results in the ingestion of the forebody boundary layer and can, therefore, result in flow separation and high flow distortion.

There are two specific objectives of this study. First, the baseline configuration and one of the inlets from a Pareto set of optimal inlets, obtained from the computational design study at zero angle of attack and zero angle of sideslip (see Ref. 1) were evaluated experimentally. The experimental inlet flow distortion at the outflow boundary was compared with the computation to ascertain the accuracy of the computations. Second, the performance of the baseline and the same optimum inlet chosen from the Pareto set of optimal inlets were evaluated experimentally at nonzero angle of attack and angles of sideslip to assess the sensitivity of the designs to these parameters.

Methodology

A computational design study[1] yielded the Pareto set of optimal designs, called optimum inlets. They were obtained based on an automated design optimization approach using two measures of high flow quality of the air: flow distortion and flow swirl. The improved inlet designs indicated a significant reduction in flow distortion at the outflow boundary compared with the baseline shape. This design study was restricted to zero angle of attack and zero angle of sideslip.

Figure 1 shows the generic air vehicle analyzed in this study. It is an ogive cylinder with a humped curved diffuser, and its dimensions are approximately one-half of the size of a typical cruise missile. The inlet is flush with the fuselage and is small compared to the overall size of the air vehicle. A trade study for a wide range of possible geometric deformations of the baseline geometry was performed.[1] According to the trade study, introduction of fins inside the channel and deformation in the shape of a fin over the inlet channel was found to be promising for achieving a lower distortion coefficient at the exit cross section of the channel. The experimental study examined one of the optimal designs from the Pareto set and also the baseline (no fins) design. The baseline and optimal inlets are shown in Fig. 2 together with the computed total pressure contours and flow streamlines. The introduction of the fins significantly reduces the flow distortion coefficient (DC) at the exit defined by the maximum deviation of the total pressure in a pie-shaped sector from the mean total pressure according to

$$\mathrm{DC}(\psi) = \max\{[\bar{p}_0 - \bar{p}_0(\phi, \psi)]/\bar{q}\}, \qquad 0 < \phi < 2\pi$$

where $\bar{p}_0$ is the area-averaged total pressure over the entire diffuser exit, $\bar{p}_0(\phi, \psi)$ is the area-averaged total pressure over a pie-shaped segment of angle $\psi = 45$ deg starting at angle ϕ at the diffuser exit, and $\bar{q}$ is the area-averaged dynamic pressure.

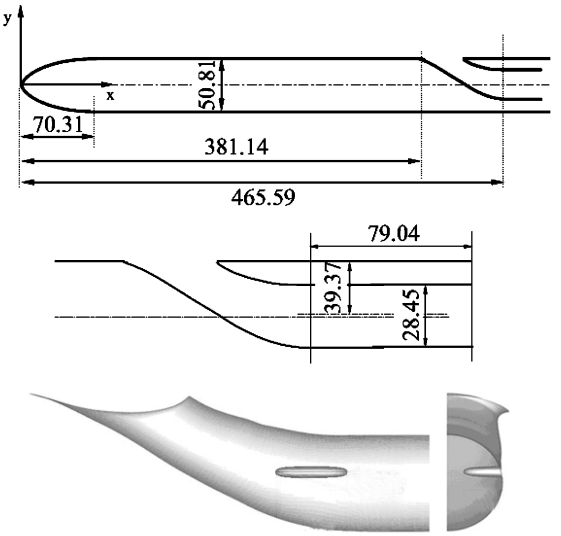

Fig. 1 Generic air vehicle forebody and inlet (dimensions in millimeters).

Presented as Paper 2004-4842 at the 22nd Applied Aerodynamics Conference and Exhibit, Providence, RI, 16–19 August 2004; received 25 January 2005; revision received 10 August 2005; accepted for publication 25 August 2005.

*Graduate Student, Department of Mechanical and Aerospace Engineering, 98 Brett Road. Member AIAA.
†Postdoctoral Fellow, Department of Mechanical and Aerospace Engineering, 98 Brett Road. Member AIAA.
‡Professor, Department of Mechanical and Aerospace Engineering, 98 Brett Road. Associate Fellow AIAA.
§Associate Professor, Department of Aeronautical and Astronautical Engineering, 104 South Wright Street. Member AIAA.

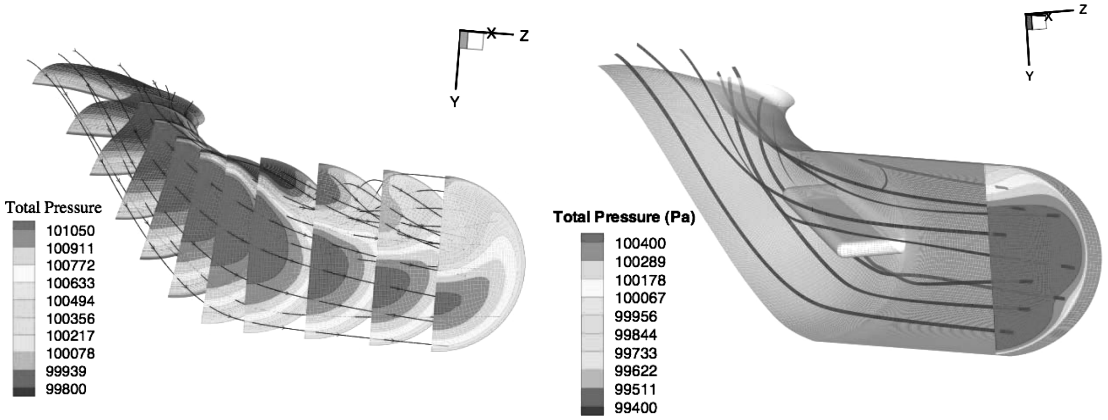

Fig. 2 Inlets: a) baseline and b) optimum.

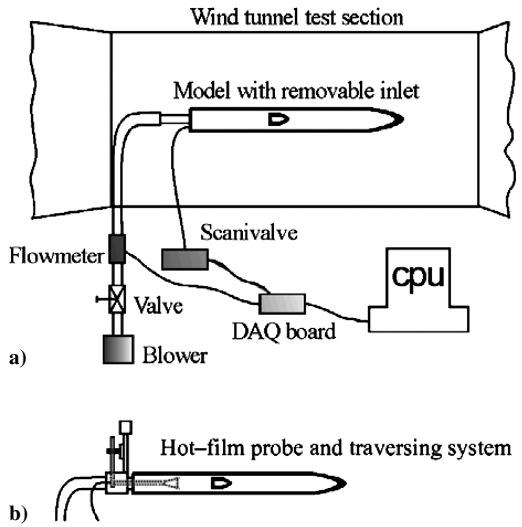

Fig. 3 Experimental setup: a) pressure differential technique scheme and b) thermal anemometry scheme.

The experimental study was conducted in the Low Speed Wind Tunnel Laboratory at Rutgers University.[2] The measurements were performed using two experimental techniques: 1) pressure differential technique using a seven-element rotating pitot rake and 2) thermal anemometry technique using hot-film probes. A typical experimental setup for pressure differential technique measurements is given in Fig. 3a. All of the data were collected using a seven-element rotating pitot rake and two static pressure taps (on the opposite sides of the tube at the pitot rake location) connected with the pressure acquisition system. Velocity information was also obtained using a hot-film probe attached to the traversing system on the top of the model, as shown in the Fig. 3b. Both the pitot rake and the tip of the hot-film sensor were located three diameters (79.04 mm, as shown in Fig. 1) downstream of the inlet exit. The accuracy of the thermal anemometry system in measuring velocity was $\pm 5\%$, whereas the accuracy of the pressure differential system was $\pm 3\%$ (Ref. 2).

Results

Computed and experimental results of the DC for the baseline and optimum inlets for zero angle of attack and zero angle of sideslip are presented, together with the computed and experimental axial velocity contours for the baseline inlet. These results are followed by the experimental DC results for nonzero angles of attack and sideslip. Computations were not performed for nonzero angles of attack and sideslip. Additional detailed experimental results for axial velocity contours and turbulence are presented in Ref. 2. Flow conditions for the computation and experiments are given in Table 1. The Mach number, flow rate, and incoming boundary-layer profiles immediately upstream of the entrance to the submerged inlet were matched for the computational and experimental studies.

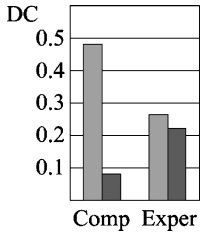

Fig. 4 Experimental and computed DC for $(\alpha, \beta) = (0, 0)$ deg: □, baseline and ■, optimum.

Table 1 Flow conditions for computational and experimental studies

Type	M_∞	Re_L^a	q^b	α, deg	β, deg
Baseline model					
Computational	0.15	1.32×10^6	0.256	0	0
Experimental	0.15	1.47×10^6	0.256	−10–10	0–10
Optimum model					
Computational	0.15	1.32×10^6	0.256	0	0
Experimental	0.15	1.45×10^6	0.256	−10–10	0–10

[a]Reynolds number at 250 mm downstream of the tip of the model.
[b]Ratio of mass flow rate at $A = A_{exit}$ to the mass flow rate that would be achieved assuming isentropic expansion from freestream conditions to sonic conditions at $A = A_{exit}$.

Zero Angle of Attack and Sideslip

The computed and experimental DCs for the baseline and optimum inlet at zero angle of attack and sideslip are shown in Fig. 4. The DC is evaluated at the engine face, that is, 3 diameters downstream of the inlet exit, using the discrete set of points corresponding to the experimental pitot survey. The computed total pressure values are interpolated to the same locations as the experiment. Numerical integration is based on Simpson's rule (see Ref. 3).

The computed and experimental DC show a similar trend, that is, the introduction of fins inside the inlet reduces the DC by creating a secondary flow that counteracts the swirl caused by the boundary-layer separation and crossflow pressure gradient.[1] The computed DC decreases by 83%, whereas the experimental DC decreases by 16%. The discrepancy between the computed and experimental DC results is explained by the axial velocity contours at the inlet exit shown in Fig. 5 inasmuch as the variation in total pressure in this case is principally due to variation in the velocity. Although both the computed and experimental velocity contours display a region of low velocity in the upper portion of the inlet associated with the separation of the boundary layer on the lower surface and formation of strong secondary flows,[1] the computed peak velocity in the lower portion of the inlet is higher than measured. The difference between the computed and experimental velocity is attributable to limitations of the turbulence model used in the computations.[2]

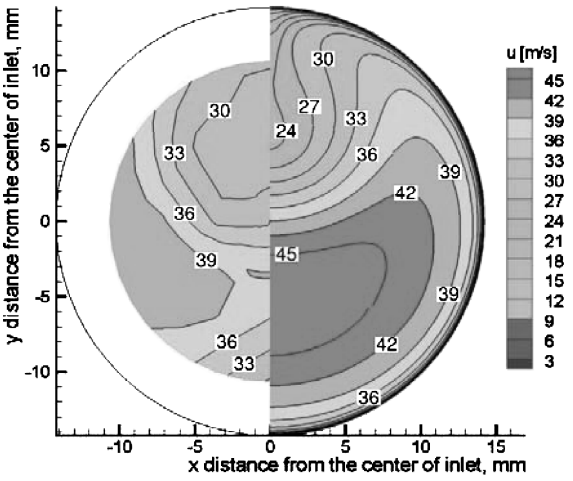

Fig. 5 Experimental and computed axial velocity for $(\alpha, \beta) = (0, 0)$ deg.

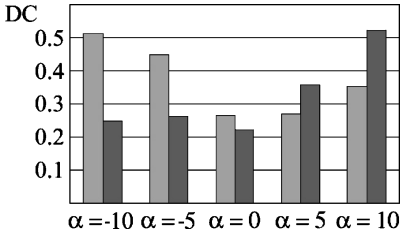

Fig. 6 Experimental DC for different angles of attack: □, baseline and ■, optimum.

Effect of the Angle of Attack

The baseline and optimum inlet flowfields at the exit plane were examined at angles of attack α from -10 to 10 deg (where model nose upward motion defines the positive increment of the angle of attack) in increments of 5 deg. As indicated in Fig. 6, the experimental DC for the optimum inlet was nearly constant for all negative angles of attack. Comparing those values to the experimental DCs for the baseline case, the improvement is evident. For the $\alpha = -10$ deg case, the calculated DC for the optimum inlet was less than one-half the value of the baseline inlet DC (0.25 compared to 0.51). Therefore, compared to the baseline inlet case, the optimum inlet DC improved by 52%. For the positive angles-of-attack cases, however, the optimum inlet displayed a higher DC than for the baseline case (32%).

Effect of the Angle of Side Slip

The baseline and optimum inlet flowfields at the exit plane were examined at angles of sideslip β of 5 and 10 deg at zero angle of attack. The addition of fins inside the optimum inlet successfully kept the high-velocity region in the lower part of the channel, creating a less distorted flow, and hence, the calculated DC showed improvement for all yaw angles for the optimum inlet compared to the baseline inlet as seen in Fig. 7. For example, the DC was reduced by 17% reduction at $\beta = 10$ deg.

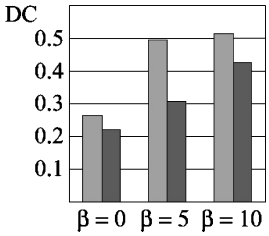

Fig. 7 Experimental DC for different angles of sideslip: □, baseline and ■, optimum.

Dynamic Data Driven Application System

The computational and experimental studies constitute an application of the Dynamic Data Driven Application System concept[4] wherein computation and experiment are used in a synergistic manner to expedite the design optimization process. The computations led to the discovery of the internal fins as a means to reduce the DC. However, the computations were only performed at zero angle of attack and sideslip due to the substantial computational cost of each simulation. The experiments were conducted at multiple angles of attack and sideslip as the incremental time and effort required to examine each additional angle of attack and sideslip was minimal.

Conclusions

Our results showed a consistent trend between computed and experimental results in reduction of the DC for the optimum inlet compared to the baseline inlet for zero angle of attack and sideslip.[5] The computed and experimental DC reduced by 83% and 16%, respectively, compared to the baseline inlet. The experimental study was further extended to investigate the dependence of the flow structure on the angle of attack and angle of sideslip. The DC improved for the optimum inlet compared to the baseline inlet for negative angles of attack (52% reduction for $\alpha = -10$ deg case) and all angles of sideslip (17% reduction for $\beta = 10$ deg case).

Acknowledgments

This research is supported by the National Science Foundation under Grant NSF-CTS-0121058 monitored by Frederica Darema, Chuan E. Chen, and Michael Plesniak.

References

[1]Taskinoglu, E., and Knight, D., "Multi-Objective Shape Optimization Study for a Subsonic Submerged Inlet," *Journal of Propulsion and Power*, Vol. 20, No. 4, 2004, pp. 620–633.

[2]Jovanovic, V., "Experimental Investigation of a Submerged Subsonic Inlet," Ph.D. Dissertation, Dept. of Mechanical and Aerospace Engineering, Rutgers Univ., New Brunswick, NJ, Oct. 2004.

[3]Recktenwald, G., *Numerical Methods with Matlab*, Prentice–Hall, Upper Saddle River, NJ, 2000.

[4]http://www.cise.nsf.gov/eia/dddas.

[5]Knight, D., Elliott, G., Jaluria, Y., Langrana, N., and Rasheed, K., "Automated Optimal Design Using Concurrent Integrated Experiment and Simulation," AIAA Paper 2002-5636, Sept. 2002.